Medicinal Chemistry Research (2023) 32:764–776
https://doi.org/10.1007/s00044-023-03036-8

MEDICINAL CHEMISTRY RESEARCH

ORIGINAL RESEARCH

Novel imino-thiazoloquinoxaline derivatives against renal cell carcinoma: less radiation-damaging approach

Nashwa H. Zaher[1] · Reham M. M. El-Hazek[1] · Mostafa G. M. El-Gazzar[1] · Walaa A. El-Sabbagh[1] · Noha A. Fadel[1]

Received: 12 December 2022 / Accepted: 8 February 2023 / Published online: 24 February 2023

Abstract

Renal cell carcinoma (RCC) is the most fatal tumor in the urinary system. Resistance development and unmet effective responses, request new anticancer agents with better therapeutic index. Ten new imino-thiazolo-quinoxaline derivatives (5a-j) were synthesized and preliminary evaluated for downregulation of Vascular Endothelial Growth Factor Receptor-2 (VEGFR-2) activity taking sorafenib as a reference drug. Compounds **5d** & **5h** showed potent inhibition to VEGFR-2 activity at IC_{50} 89.35 nM & 60.64 nM, respectively, then they both were further evaluated in-vitro against urinary bladder cancer cell line T-24 taking sorafenib as a reference drug. Compound **5h** displayed nearly anticancer activity to sorafenib against T-24 cell line in all concentrations tested except at concentration 10 µM where it highly suppressed cell viability to 6.71 % compared to 15.15% of sorafenib. Compound **5h** was then evaluated for its ameliorative efect against radiation induced renal tissue injury. Assessment of pro-angiogenic (VEGFR-2), pro-fibrotic (transforming growth factor-beta 1 (TGF-β1)) and apoptotic (caspase-3) markers, as well as histopathological examinations were performed on kidney of irradiated mice. Results showed ability of compound **5h** to downregulate VEGFR-2 activity and its cytotoxic effect against RCC, in addition to mitigation of radiation induced renal tissue injury. Ethyl imino-thiazoloquinoxaline carboxylate derivative **5h** showed a potential cytotoxic activity against RCC and could be considered a promosing alleviative candidate when employed post radiotherapy regimen.

Graphical Abstract

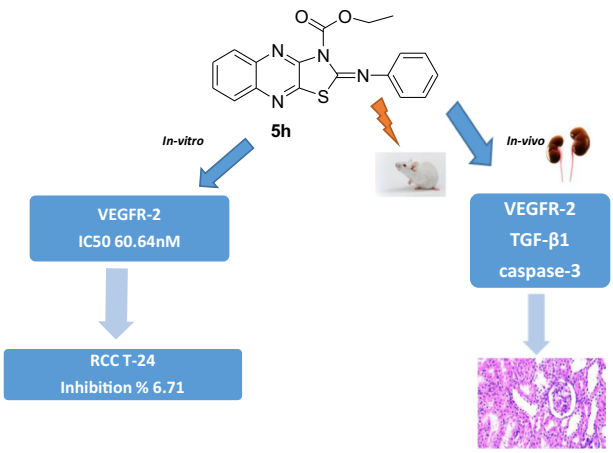

Supplementary information The online version contains supplementary material available at https://doi.org/10.1007/s00044-023-03036-8.

✉ Nashwa H. Zaher
nashwazah@hotmail.com

[1] Drug Radiation Research Department, National Center for Radiation Research & Technology (NCRRT), Egyptian Atomic Energy Authority, Cairo 11787, Egypt

Keywords Thiazoloquinoxaline · renal cell carcinoma · VEGFR-2 · radiation

Introduction

The most prevalent type of kidney cancer, renal cell carcinoma (RCC), develops from the tubular epithelium. The incidence of kidney cancer in men is higher than that in women, with peak age at 60–70 years [1]. Treatment landscape for RCC has evolved dramatically, including; targeted therapeutics, immune-checkpoint inhibitors and/or radiotherapy. RCC is perceived to be a radioresistant malignancy as local renal tumor control was achieved but with exposure to high dose of ionizing radiation, and is often restricted due to damaging response observed in the surrounding normal tissues [2]. Ionizing radiation induces damage of the DNA double strand, persuading a molecular cascade of inflammation, cellular senescence and endothelial cell death may occur, leading to apoptosis and interstitial fibrosis [3]. Recent occurrences in the RCC microenvironment, disease biology and resistance mechanisms, formed the basis for attempts to combine radiotherapy with targeted anti-angiogenic therapeutics such as tyrosine kinase inhibitors (TKIs) for better therapeutic outcomes [4].

As one of the hallmarks of cancer, angiogenesis plays a vital role in tumor development and proliferation, and has long been a prospective therapeutic target in RCC [5]. Sorafenib (Nexavar)® is an orally active multi-kinase inhibitor of tumor-cell proliferation and angiogenesis. It targets several subtypes of tyrosine kinase, including vascular endothelial growth factor receptor (VEGFR) and platelet-derived growth factor receptor (PDGFR), which are crucial pro-angiogenic factors in most tumors. In December 2005, sorafenib has been considered the first targeted chemical drug licensed by FDA for treatment of advanced RCC [6]. Sorafenib administration was reported to have many side effects that negatively affecting the patients' quality of life, in addition to resistance development [7]. Since then, other tyrosine kinase inhibitors targeting VEGFR and PDGFR have been approved for the treatment of RCC, such as bevacizumab, sunitinib, axitinib, cabozanitinib, lenvatinib, and pazopanib [8]. A potential new approach for long term management of RCC is combination therapy [9] where more than one drug is used and the dual targeting strategy which targets more than one receptor is applied [10]. Despite the fact that targeted therapies are now the standard treatment option for renal cancer, some of RCC patients are primarily resistant to them, showing neither clinical benefits nor disease stabilization [11, 12].

There is always an urgent need for exploring new RCC candidates with improved efficacy and selectivity to counteract resistance development, limited durable responses and hazards side effects. Quinoxaline is an eminent moiety for its versatile spectrum of biological activities [13]. It is well known that these compounds could compact infectious and non-infectious diseases [14], in addition to their anti-cancer properties [15, 16]. They are also considered as potent VEGFR-2 inhibitors compared to sorafenib [17].

Based on the aforementioned background, and in continuation to our work in exploring new anticancer entities targeting VEGFR-2 [18], the current study was constructed to design and synthesize a novel series of imino-thiazoloquinoxaline derivatives targeting VEGFR-2 and to assess its potential cytotoxic activity against RCC. The efficacy of the most potent compound was then evaluated for its ability to attenuate normal tissue injury induced after irradiation by analyzing its in-vivo capacity to suppress the apoptotic and fibrotic markers, as well as the angiogenic factor VEGFR-2.

Rationale and design

Downregulating VEGFR-2 signaling cascade is verified as the most proficient mechanism of action for novel chemotherapeutics in advanced RCC [19, 20]. Recently, many drugs are approved by FDA as controlling VEGFR-2 enzyme and inhibiting angiogenesis. Axitinib (Inlyta ®); one of the recent 3rd generation approved drugs in RCC treatment exerting activity against TKIs, c-Kit and PDGRG-β. Clinical trials proved its efficacy compared to sorafenib with better PFS [21]. However, cardiotoxicity, hypertension and fatigue were the most prominent side effects leading to axitinib discontinuation [22]. Despite emergence of such drugs as promising angiogenesis inhibitors with much improvement in RCC patients' outcomes and survival rates, cancer resistance develops due to downstream activation of signaling pathway. In addition, the adverse effects caused by these therapeutics are more hazardous, affecting negatively patients' health. There is always a need to explore new therapeutics.

Quinoxalines are attractive targets for exploring new VEGFR-2 inhibitors and selective RCC drugs [23]. The following four major pharmacophoric features are needed to occupy four regions in the active binding site of VEGFR-2 in order to downregulate its activity [24]; 1-Heteroaromatic ring to occupy the hinge region. 2- central aromatic linker to occupy the Gatekeeper region. 3- Hydrogen bond donor-hydrogen bond acceptor (HBD-HBA) to interact with Glu 883 and Asp 1044 in DFG domain. 4- Terminal lipophilic

moiety to occupy the allosteric lipophilic pocket. According to the above mentioned verdicts, along with applying bioisosteric modification approach, series of thiazoloquinoxaline derivatives was designed and synthesized comprising required fragments for VEGFR-2 downregulation, taking axitinib as an example (Fig. 1). For occupying the hinge region, quinoxaline ring acts as the heteroaromatic moiety, expecting to offer more binding interactions than pyridine ring. This comes in accordance with Yu et al. [25] who reported that substitution of sorafenib pyridine ring and urea, contributed in more kinase targeting effect. Thiazole ring is the central aromatic linker in our designed compounds, to occupy the gate keeper region, such that 1,3-substituted ring was reported to show superior activity in VEGFR-2 inhibition [26]. Thiazole ring and / Or its substitutions along with central imine, supposed as HBD-HBA pharmacophore, aiming to form H- bonds for inhibitory activity against VEGFR-2. Finally, the terminal phenyl ring is nominated to occupy the allosteric lipophilic pocket [24].

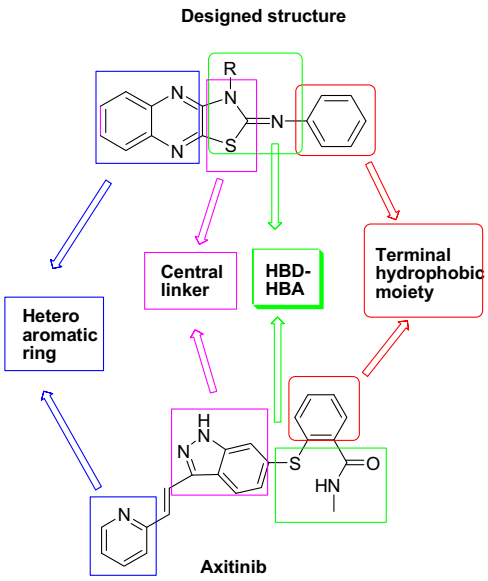

Fig. 1 Main structural requirements for VEGFR-2 inhibition using axitinib as an example

Results and discussion

Chemistry

The novel synthesized compounds were prepared according to the pathways described in Scheme 1, the phenyl isothiocyanate **(1)** was refluxed with different substituted amines; methylamine, ethylamine, allylamine, propyl amine, isopropyl amine, butyl amine, isobutyl amine, ethyl carbamate, cyclohexyl amine and benzyl amine **2 (a-j)**, respectively, in ethanol for 8 h and yielded the reported thiourea derivatives **3 (a-j)**, respectively. [27–30]. Then by further reaction of compounds **3 (a-j)** with 2,3-dichloroquinoxaline **(4)** in ethanol for 8 h gave the target compounds **5 (a-j)**, respectively in good yields. Scheme 1.

All the assigned structures for the target compounds **5 (a-j)** were confirmed by IR, ^{1}H NMR, ^{13}C NMR, mass spectra and microanalytical data. Their structures were characterized by the disappearance of the characteristic C = S and NH bands and signals of the intermediate compounds **3 (a-j)** in all the spectral data. In addition to appearance of new bands for the C = N in the IR spectra of compounds **5 (a-j)** at range 1645–1688 cm^{-1}. Also disappearance of NH signals in ^{1}H-NMR spectra exchangeable with D_2O. Moreover, the presence of some characteristic signals in the ^{1}H-NMR spectra for compounds **5 (a-j)** as exhibition of singlet signal at δ 3.88 ppm for the methyl protons of compound **(5a)**. Triplet upfield signals were displayed at δ 1.51 and 1.11 ppm assigned for the methyl group of compounds **(5b)** and **(5d)**, respectively. Doublet signals were exhibited at δ 5.19 and 1.28 ppm attributed to the N-$\underline{CH_2}$ group of **(5c)** and the two methyl groups **(5e)**, respectively. Also the appearance of triplet signals at δ 1.23 and 1.29 ppm for the methyl protons of **(5f)** and **(5h)**, respectively. Doublet signals were revealed at δ 1.12, 1.13

Scheme 1 Synthetic route of compounds 5(**a-j**)

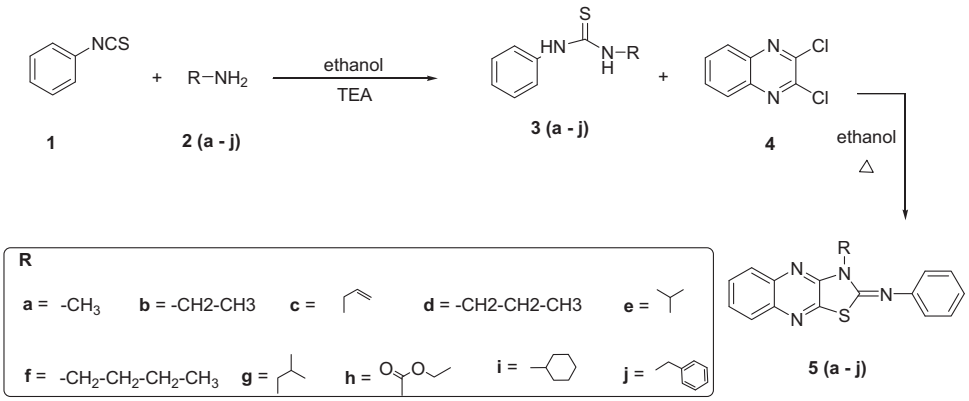

Table 1 In-vitro VEGFR-2 inhibitory activity

Compound	VEGFR-2 IC_{50} (nM)[a]
5a	349.60 ± 15
5b	168.70 ± 7.52
5c	269.05 ± 12.03
5d	89.35 ± 3.40
5e	181.62 ± 8.12
5f	201.30 ± 9.00
5g	191.06 ± 8.54
5h	60.64 ± 2.70
5i	94.73 ± 4.23
5j	156.02 ± 6.70
Sorafenib	51.41 ± 2.30

[a]IC50 values are the mean ± S.D (standard deviations) of three experiments

ppm for the two methyl groups **(5g)**. Multiplet signals were displayed at range 1.19–2.98 ppm for the protons of the cyclohexane ring **(5i)**. Singlet signal at 4.81 ppm assigned for the CH_2-phenyl **(5j)**.

Additionally, the ^{13}C-NMR spectra for compounds **5 (a-j)** showed the appearance of signals at range 136.11–136.85 ppm for the newly formed N = C-S. Exhibition of signals at δ 145.68–150.69 ppm for the C-N, 156.05–159.04 ppm for C = N. Displaying of most downfield signals at range 161.16–163.34 ppm ascribed for N = C-N. This showed that the NH and C = S groups of the thiourea in compounds **3 (a-j)** were incorporated by cyclization to form the 5-membered thiazole ring in compounds **5 (a-j)**. Moreover, the mass spectra and microanalytical data of compounds **5 (a-j)** were in agreement with their postulated structures.

Pharmacology/biology

In-vitro studies

The selectivity of the newly synthesized compounds towards VEGFR-2 was assessed and compared to that of sorafenib as a reference drug. The results were expressed as 50% inhibition concentration value (IC50, determined in triplicate) as shown in Table 1.

Compound ethyl carboxylate derivative **5h** offered the maximum inhibitory activity followed by propyl derivative **5d** with IC50 value 60.64 and 89.35 nM respectively, compared to that of sorafenib (IC50 = 51.41 nM). This comes in accordance with El-Adl et al. [31] who reported that ethyl carboxylate derivative was the most potent in VEGFR-2 inhibition among a series of different derivatives within the same study. Also, Abuelizz et al. [32] reported

Table 2 In-vitro anticancer activity of compounds 5h, 5d and sorafenib against T-24 (urinary bladder cancer) cell line

Concentration (μM)	Sorafenib Viability%	Compound 5h Viability %	Compound 5d Viability %
0.01	101.60 ± 0.74	98.14 ± 1.02	98.77 ± 0.13
0.1	99.49 ± 1.58	98.20 ± 0.88	99.24 ± 1.56
1	96.13 ± 3.08	98.38 ± 0.94	98.78 ± 0.08
10	15.15 ± 0.31	6.71 ± 1.10	98.32 ± 0.69
100	0.55 ± 0.16	0.43 ± 0.12	92.29 ± 2.11

Data are expressed as mean ± S.D (standard deviations) of three experiments

that propyl derivative was very potent among other derivatives at inhibiting VEGFR-2.

Thereafter, compounds **5h** and **5d** were selected to be evaluated for their in-vitro cytotoxic activity against RCC (T-24) by SRB assay method. The cytotoxic efficacy of the two compounds was compared to that of sorafenib. The data demonstrated the cell viability (surviving fraction) and drug concentration was shown in Table (2). Notably, compound **5h** exhibited a potent cytotoxic activity against renal cell line with **IC50 = 4 μM**, which is nearly equivalent to that of sorafenib (**IC50 = 4.43 μM**), while compound **5d** displayed **IC50 > 100 μM**. RCC is a notoriously hypervascularized tumor that is prone to distant metastasis. RCC is characterized by the loss of von Hippel-Lindau tumor suppressor protein, resulting in up-regulation in the tumorigenic hypoxia-responsive gene transcription of VEGF and PDGF. These factors promote angiogenesis as well as tumor proliferation by activating tyrosine kinase receptors VEGFR and PDGFR [5, 33]. Herein, the newly synthesized **Ethyl 2-(phenylimino)thiazolo[4,5-b]quinoxaline-3(2H)-carboxylate 5h** counteracted the pro-angiogenic VEGFR-2 activation and confers a cytotoxic impact on the renal cell line. This comes in accordance with Hajri et al. [34], who reported synthesis of quinoxaline ethyl carboxylate series which demonstrated substantial antiproliferative activity. Accordingly, compound **5h** was selected to investigate its impact on the renal tissue of irradiated mice.

In-vivo studies

Radiation toxicity to healthy tissue limits the applied doses of radiotherapy and thereby, limits its therapeutic success [3]. In normal tissue, radiation triggers a molecular cascade leading to persistent alterations in the microenvironment, comprising features of hypoxia, angiogenesis, apoptosis, and fibrogenesis [35]. Accordingly, in-vivo study was carried out to explore the potential of compound **5h** to interfere with such detrimental cascade and to maintain normal renal function post irradiation exposure. According to the

previous experimental and clinical trials, the mechanism of action of VEGFR-TKIs pathways provides a strong rationale for its combined use post- radiotherapy [4]; ionizing radiation up-regulates the expression of growth factors in tumor cells, promoting tumor angiogenesis and proliferation, thereby contributing to the protection of tumor blood vessels from radiation-mediated cytotoxicity and subsequently to tumor radioresistance [36, 37].

In the current study, mice exposed to 8 Gy of radiation, exhibited a state of acute kidney injury and renal biochemical changes, as demonstrated by the assessed biochemical parameters and histopathological examinations. As shown in Table 3, irradiation of mice elevated the serum urea by nearly 5-fold and increased the serum creatinine by 33%, which revealed considerable impairment of renal function [38]. Notably, oral administration of sorafenib decreased the serum urea and creatinine levels by 76% and 18%, respectively, while treatment with compound **5h** prominently reduced them by 87% and 28%, respectively, as compared to the IR group.

Table 3 Effect of compound 5h and sorafenib on the kidney functions of irradiated mice

Groups / parameters	Urea	Creatinine
Normal	5.57 ± 0.72	0.605 ± 0.018
Irradiated (8 Gy)	33.25$^{\#}$ ± 2.58	0.805$^{\#}$ ± 0.027
IR + Sorafenib (50 mg/kg)	8.01* ± 0.98	0.661* ± 0.031
IR + Compound 5 h (50 mg/kg)	4.42* ± 0.24	0.577* ± 0.032

Values are expressed as mean values ± SEM

$^{\#}$Significant different ($p < 0.05$) compared to normal group

*Significant different ($p < 0.05$) compared to irradiated group

Such results of renal function are consistent with that of the histopathological examinations (Fig. 2); tissue sections of normal group (Fig. 2A) showed normal histological structure characterized by circumscribe glomeruli with normal structure of capillary tufts and bowman's capsule. Renal tubules of both proximal and distal convoluted tubules showed intact epithelial lining and regular arrangement (**score 0**). On the other side, tissue sections of IR group (Fig. 2B) showed atrophy of glomeruli with shrinkage of capillary tufts, degeneration of renal tubular epithelial lining appeared in form of swelling and granularity of its cytoplasm, intra-tubular albumin eosinophilic casts, focal aggregation of mononuclear cells mainly lymphocytes and macrophages, and interstitial edema with tubular epithelial cell necrosis and apoptosis <75% (**score 4**).

The group exposed to radiation and treated with sorafenib (Fig. 2C) revealed moderate histological changes in renal tubular epithelial lining appeared in form of swelling of tubular epithelial lining with intra-luminal albuminus casts and tubular epithelial cells showed degeneration, necrosis and apoptosis <25% (score 2), while, the IR group treated with compound **5h** (Fig. 2D) showed mild histological changes in renal tubular epithelial lining appeared in form of mild swelling and granularity of its cytoplasm with cystic dilatation of some tubules. Intra-tubular albuminus eosinophilic casts without significant necrosis or apoptosis were seen (score 1). These results revealed that the newly synthesized compound **5h** highly alleviates

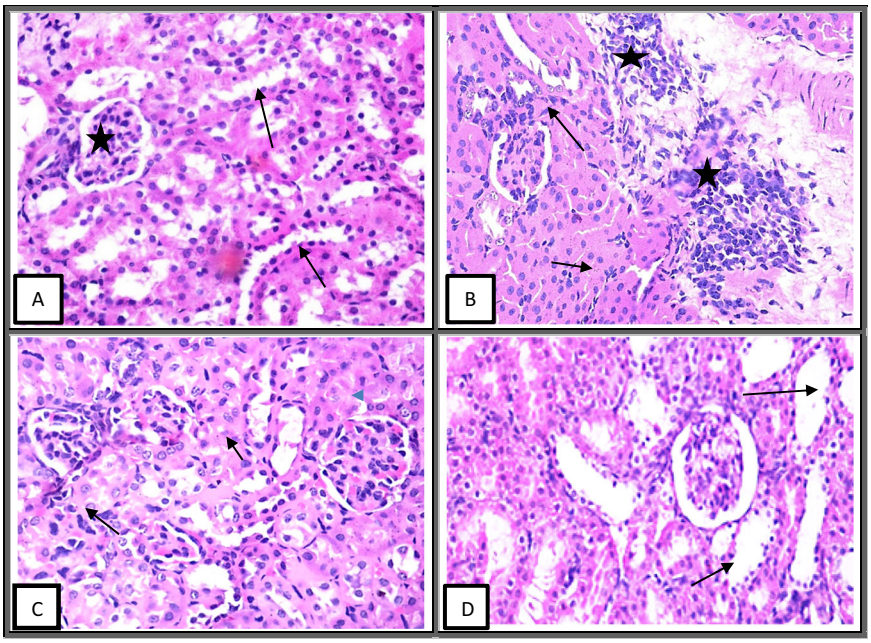

Fig. 2 Photomicrograph of renal tissue section (H&EX200) of (**A**) normal group showed intact structure of glomeruli (star) with regular arrangement of tubular epithelial lining (arrow) (**B**) irradiated (IR (8 Gy)) group showed focal aggregation of mononuclear cells (star) with tubular epithelial cell necrosis (arrow) (**C**) IR + sorafenib (50 mg/kg) treated group showed swelling of tubular epithelial lining with apoptotic cells (arrow) (**D**) IR + compound **5h** (50 mg/kg) treated group showed mild swelling of tubular epithelial lining with cystic dilatation of some tubules (arrow)

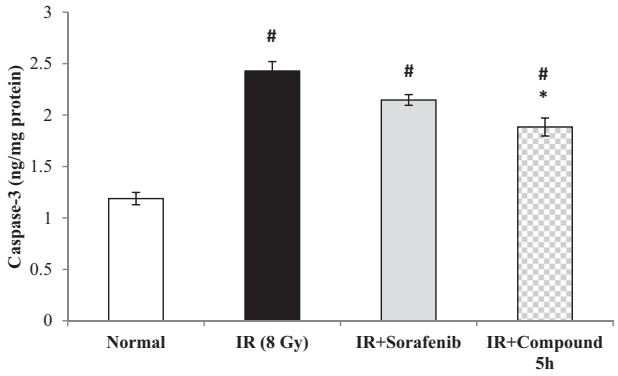

Fig. 3 Effect of compound **5h** (50 mg/kg) and sorafenib (50 mg/kg) on the concentration of caspase-3 in kidney tissue of irradiated mice. Values are expressed as mean values ± SEM. #Significant different ($p < 0.05$) compared to normal group. *Significant different ($p < 0.05$) compared to irradiated group

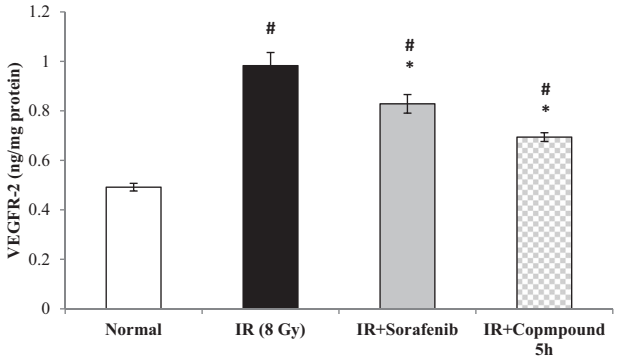

Fig. 4 Effect of compound **5h** (50 mg/kg) and sorafenib (50 mg/kg) on the concentration of VEGFR-2 in kidney tissue of irradiated mice. Values are expressed as mean values ± SEM. # Significant different ($p < 0.05$) compared to normal group. *Significant different ($p < 0.05$) compared to irradiated group

radiation-induced harm features. To validate such ameliorative effect, the molecular apoptotic, angiogenic and fibrotic markers were then estimated in kidney tissue.

Radiation-induced tissue injury is initially marked by the direct cytotoxic action of reactive oxygen species (ROS) on the DNA that led to endothelial cell damage, vascular permeability and edema, with subsequent infiltration and accumulation of macrophages. The induced DNA damage is thought to be the main contributor in triggering the apoptosis cascade that results in tissue destruction [39]. Exposure to radiation was reported to induce imbalance between the pro-and anti-apoptotic proteins, leading to activation of the apoptosis cascade in renal cells [40]. Herein, the data showed in Fig. (3) revealed that exposure to radiation increased the apoptotic protein caspase-3 concentration in kidney by nearly 1-fold, as compared to the normal group. This was in line with the study of Özyurt et al. [41] as they reported that irradiation exposure enhanced the release of the apoptotic factor caspase-3 in kidney and bladder tissues which led to tissue damage. Treatment with sorafenib suppressed the caspase-3 by 12%, yet, it did not show a significant difference from the IR group, while compound **5h** significantly suppressed the kidney content of caspase-3 by 22%, thus exerting an anti-apoptotic effect.

In response to the apoptosis of vascular endothelial cells triggered by radiation, endothelial cells surviving factors such as VEGF was stimulated as a self-protecting factor, however, accumulation of radiation damage and endothelial cells death perpetuate a non-healing tissue response [35]. In this context, the current study assessed the potential of compound **5h** to suppress the VEGFR-2 activation in renal tissue after radiation exposure. Our results showed that exposure to radiation up-regulated VEGFR-2 expression by nearly onefold, as compared to the normal group (Fig. 4). Such results were in agreement with the study of El-Gazzar et al. [18], which postulated that irradiation exposure upsurges VEGFR-2 protein expression in hepatic tissue. On the other side, oral administration of sorafenib suppressed the VEGFR-2 content in kidney by 16%, while treatment with compound **5h** offered a higher percentage of inhibition (30%), as compared to the IR group (Fig. 4).

Mechanistically, the increased oxygen consumption due to radiation activation of macrophages contributes to the development of hypoxia which further up-regulates the production of the pro-angiogenic VEGF and pro-fibrotic transforming growth factor-beta (TGF-β), which in turn stimulates tissue angiogenesis and fibrogensis [35, 42]. It was clear that angiogenesis and fibrogenesis have some common pathological mechanisms and pathways, and thereby anti-angiogenic therapies were considered as a target therapy for fibrosis [43].

Development of renal fibrosis is a dose limited complication of radiotherapy; the sustained activation of macrophages and myofibroblast after radiation exposure seemed to be crucial to renal fibrosis as both inflammatory cells synthesize and secrete the pro-fibrotic TGF-β1. Besides, radiation-induced apoptosis of vascular endothelial cells lowered the amount of intrinsic cells responsible for appropriate renal function and hastening the fibrosis process [44]. In the current investigation, this was demonstrated as exposure to radiation boosted the production of the TGF-β1 by nearly onefold, as compared to normal group (Fig. 5). Similarly, the study of Mostafa et al. [45] reported that irradiation stimulated the renal TGF-β1/smad signaling pathway and precipitated nephritis in rats.

The current results showed that oral administration of sorafenib suppressed the elevated kidney content of TGF-β1 by 30%, while treatment with compound **5h** highly suppressed it by 43%, indicating a significant difference from sorafenib treated group and revealing its capabililty to hamper the process of renal fibrosis.

Remarkably, the in-vivo studies revealed the superiority of ethyl imino-thiazoloquinoxaline carboxylate derivative **5h** as promising approach to guard against radiation-induced kidney harm. This comes in allignment with the study of Ghorab et al. [46], who reported synthesis of ethyl carboxylate series with radioprotective and anticancer effect.

Molecular docking

In silico evaluation using molecular docking was performed in order to confirm and interpret the preliminary VEGFR-2 inhibition results for the newly synthesized compound 5 h. MOE software was used with human VEGFR-2 (PDB: 1ASD). Docking study was performed for the most active compound Ethyl 2-(phenylimino)thiazolo[4,5-b]-quinoxaline-3(2H)-carboxylate (**5h**), within the active binding site of VEGFR-2 in order to have more perception about the binding mode, taking into consideration main pharmacophoric features required for binding in order to downregulate VEGFR-2 activity as reported by Lee et al. [24].

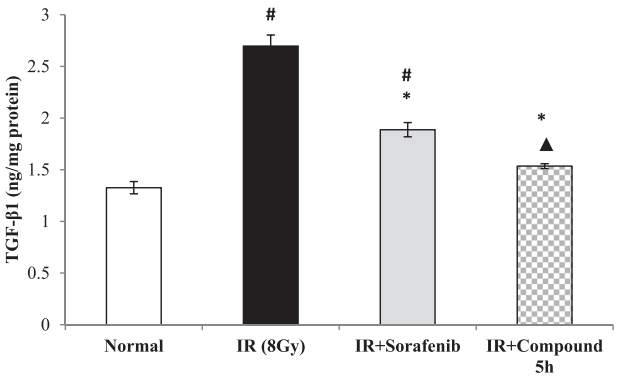

Fig. 5 Effect of compound **5h** (50 mg/kg) and sorafenib (50 mg/kg) on the concentration of TGF-β1 in kidney tissue of irradiated mice. Values are expressed as mean values ± SEM. # Significant different ($p < 0.05$) compared to normal group. *Significant different ($p < 0.05$) compared to irradiated group. ▲Significantly different ($p < 0.05$) compared to sorafenib group

It could be noticed that structure of Ethylcarboxylate derivative **5h** occupies mainly the catalytic site of VEGFR-2 receptor, which potentially could be reason for its selectivity. It fits through the following binding interactions (Fig. 6), with scoring energy −6.273 compared to −7.792 of axitinib (supplementary): Quinoxaline ring occupies hinge region. Pyrimidine of the quinoxaline occupied the gatekeeper region as central aromatic linker. At the same time, it forms arene binding interaction with Asp 1044 in DFG domain (HBD-HBA pharmacophore). Sulfur of thiazole ring forms additional main H- bond with Glu 885 in DFG domain. Thiazole ring forms arene interaction with Leu 889. Terminal phenyl ring occupies the allosteric lipophilic pocket.

Conclusion

In this work, ten new imino-thiazolo-quinoxaline derivatives (5a-j) were synthesized and structurelly verified. The newely obtained compounds (5a-j) were evaluated in-vitro

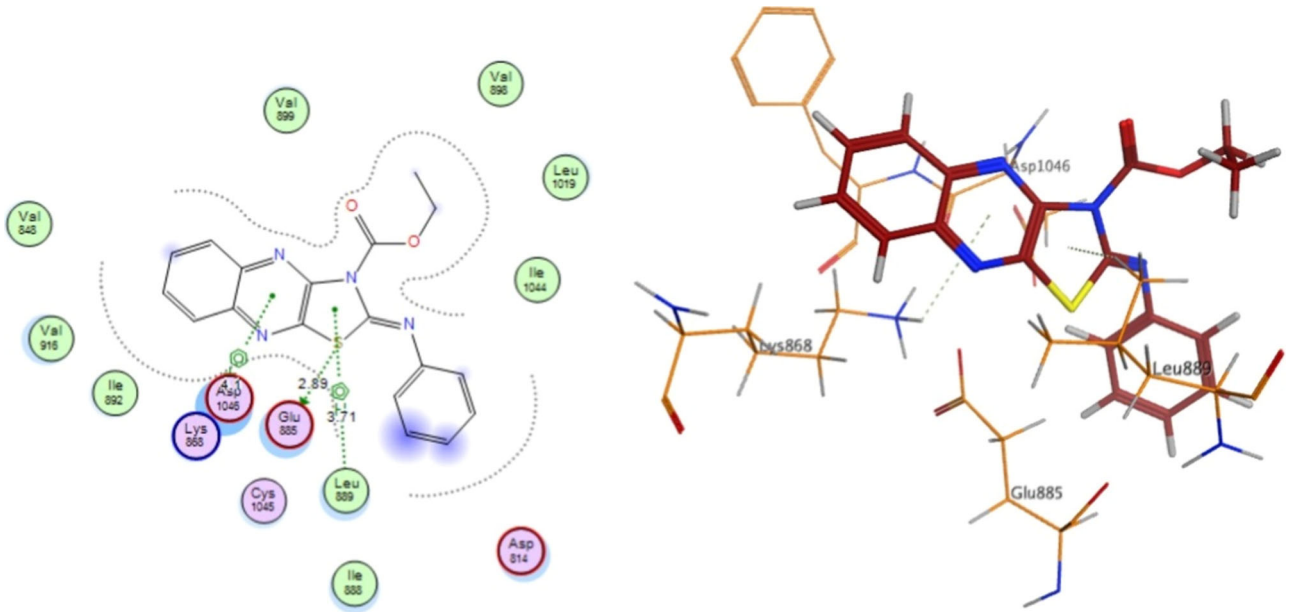

Fig. 6 2D and 3D binding interactions of compound **5h** into VEGFR-2 (PDB: 4ASD)

as VEGFR-2 inhibitors. The most potent compounds **5d & 5h** were subjected for assessment against RCC cell line. Accordingly, compound **5h** showed a potent cytotoxic activity and was then evaluated for its conservative effect against radiation induced renal damage. Compound **5h** was found to diminish the elevated apoptotic, angiogenic and fibrotic mediators in irradiated mice. Collectively, the current study revealed the potential dichotomous impact of the newly synthesized **Ethyl 2-(phenylimino)thiazolo[4,5-b] quinoxaline-3(2H)-carboxylate (5h)** as down regulator to VEGFR-2 activity and a cytotoxic agent against RCC. Also, compound **5h** has salutary impact in lowering radiation-induced deletrious effects on renal tissue, showing its promising role when employed post radiotherapy regimen.

Experimental

Chemistry

General

Uncorrected melting points were recorded using a Stuart melting point device (Stuart Scientific, Redhill, UK) and were transported in open capillary tubes. The infrared (IR) spectra of the substances were captured using an FTIR Shimadzu spectrometer (Shimadzu, Tokyo, Japan). TMS was utilised as an internal Standard and DMSO-d6 as the solvent for recording 1H NMR and 13 C NMR spectra with a Bruker (400 MHz for 1H NMR and 100 MHz for 13 C NMR) spectrometer (see supplementary data). On the HP Model MS-5988, mass spectra were conducted (Hewlett Packard, Palo, Alto, California, USA). For acquiring the results of the microanalyses, a Carlo Erba 1108 Elemental Analyzer (Heraeus, Hanau, Garmany) was employed. In order to check the completion of the reaction, pre-coated SiO_2 gel (HF254, 200 mesh) aluminum plates (Merk, Daemstadt, Germany) were employed as the TLC.

General procedure for synthesis of N-(3-substituted-thiazolo[4,5-b]quinoxalin-2(3H)-ylidene)aniline 5(a–j)

A mixture of **phenylisothiocyanate 1** (0.54 gm, 0.004 mol) and the appropriate substituted amines **2 (a–j)** (0.004 mol) was refluxed in ethanol for 5 h in the presence of 5 drops triethylamine to give the 1-substituted-3-phenylthiourea derivatives **3 (a–j)** [25–28], respectively. which were then refluxed with 2,3-dichloroquinoxaline **4** (0.79 gm, 0.004 mol) in ethanol for 8 h. The reaction mixture was cooled, then the precipitated solid was filtered, washed with ethanol, dried and crystallized from dioxane to afford compounds **5(a–j)**, respectively.

N-(3-Methylthiazolo[4,5-b]quinoxalin-2(3H)-ylidene)aniline (5a) Yield 72 %; m.p.; 161–163 °C; IR (KBr,cm^{-1}): 3094 (CH arom.), 2945, 2835 (CH aliph.), 1653 (C=N); ^{1}H NMR (DMSO-d_6, δ, ppm): 3.88 (s, 3H, CH_3), 6.46 (d, 2H, 2CH, $J = 8.00$ Hz), 6.94 (t, H, CH, $J = 8.36$ Hz), 7.06–7.22 (m, 6H, Ar-H). ^{13}C NMR (DMSO-d_6, δ, ppm): 31.24 (CH_3), 123.08 (2), 124.38, 127.01, 127.87, 129.59, 129.92, 130.61 (2), 136.85 (N=C-S), 137.73, 140.89, 148.77 (C-N), 157.46 (C=N), 162.82 (N=C-N). MS (m/z): 292 (M^+). Analysis calculated for: $C_{16}H_{12}N_4S$ (292): C, 65.73; H, 4.14; N, 19.16, found: C, 65.42; H, 4.33; N, 19.39.

N-(3-Ethylthiazolo[4,5-b]quinoxalin-2(3H)-ylidene)aniline (5b) Yield 81 %; m.p.; 172–174 °C; IR (KBr,cm^{-1}): 3083 (CH arom.), 2952, 2839 (CH aliph.), 1677 (C=N); ^{1}H NMR (DMSO-d_6, δ, ppm): 1.51 (t, 3H, CH_3, $J = 1.72$ Hz), 4.81-4.89 (m, 2H, CH_2), 7.27 (d, 2H, 2CH, $J = 16.48$ Hz), 7.50 (t, H, CH, $J = 8.28$ Hz), 7.74–7.98 (m, 6H, Ar-H). ^{13}C NMR (DMSO-d_6, δ, ppm): 13.84 (CH_3), 44.84 ($\underline{C}H_2$-CH_3), 121.26 (2), 124.40, 126.01, 127.98, 129.64, 129.84, 130.50 (2), 136.46 (N=C-S), 137.60, 139.93, 147.52 (C-N), 159.04 (C = N), 163.34 (N=C-N). MS (m/z): 306 (M^+). Analysis calculated for: $C_{17}H_{14}N_4S$ (306): C, 66.64; H, 4.61; N, 18.29, found: C, 67.03; H, 4.73; N, 18.03.

N-(3-Allylthiazolo[4,5-b]quinoxalin-2(3H)-ylidene)aniline (5c) Yield 76 %; m.p.; 202–204 °C; IR (KBr,cm^{-1}): 3063 (CH arom.), 2915, 2830 (CH aliph.), 1664 (C=N); ^{1}H NMR (DMSO-d_6, δ, ppm): 5.19 (d, 2H, N-CH_2, $J = 2.36$ Hz), 5.73-5.81 (m, 2H, CH_2), 5.90-5.98 (m, H, CH), 7.40-7.87 (m, 9H, Ar-H). ^{13}C NMR (DMSO-d_6, δ, ppm): 46.84 ($\underline{C}H_2$-CH), 119.69 (CH=$\underline{C}H_2$), 123.34 (2), 126.28, 126.41, 129.90 (2), 129.98, 130.37 ($\underline{C}$H=CH_2), 133.50 (2), 136.11 (N=C-S), 136.35, 136.51, 148.47 (C-N), 158.45 (C=N), 161.82 (N = C-N). MS (m/z): 318 (M^+). Analysis calculated for: $C_{18}H_{14}N_4S$ (318): C, 67.90; H, 4.43; N, 17.60, found: C, 67.74; H, 4.71; N, 17.38.

N-(3-Propylthiazolo[4,5-b]quinoxalin-2(3H)-ylidene)aniline (5d) Yield 84 %; m.p.; 192–194 °C; IR (KBr,cm^{-1}): 3089 (CH arom.), 2910, 2812 (CH aliph.), 1645 (C=N); ^{1}H NMR (DMSO-d_6, δ, ppm): 1.11 (t, 3H, CH_3, $J = 15.08$ Hz), 1.83–1.95 (m, 2H, $\underline{C}H_2$-CH_3), 4.26 (t, 2H, N-CH_2, $J = 7.00$ Hz), 7.17 (d, 2H, $2CH_2$, $J = 7.48$ Hz), 7.42-7.66 (m, 7H, Ar-H). ^{13}C NMR (DMSO-d_6, δ, ppm): 11.63 (CH_3), 21.21 ($\underline{C}H_2$-CH_3), 42.74 ($\underline{C}H_2$-CH_2-CH_3), 120.77 (2), 126.28, 126.41, 129.90, 129.98, 130.37, 133.50 (2), 136.11 (N=C-S), 136.35, 136.51, 148.49 (C-N), 156.25 (C=N), 163.32 (N=C-N). MS (m/z): 320 (M^+). Analysis calculated for: $C_{18}H_{16}N_4S$ (320): C, 67.47; H, 5.03; N, 17.49, found: C, 67.22; H, 4.85; N, 17.16.

***N*-(3-Isopropylthiazolo[4,5-b]quinoxalin-2(*3H*)-ylidene)aniline (5e)** Yield 87 %; m.p.; 223–225 °C; IR (KBr,cm^{-1}): 3078 (CH arom.), 2905, 2818 (CH aliph.), 1680 (C=N); ^{1}H NMR (DMSO-d_6, δ, ppm): 1.28 (d, 6H, $2CH_3$, $J = 13.72$ Hz), 2.41–2.47 (m, H, N-CH), 7.52–8.04 (m, 9H, Ar-H). ^{13}C NMR (DMSO-d_6, δ, ppm): 20.89 (2) (2 CH_3), 55.54 (CH_3-CH-CH_3), 121.04 (2), 123.47, 123.68, 126.40, 129.91, 130.01, 130.44 (2), 136.21 (N=C-S), 136.32, 136.65, 145.68 (C-N), 156.31 (C=N), 162.85 (N=C-N). MS (m/z): 320 (M^+). Analysis calculated for: $C_{18}H_{16}N_4S$ (320): C, 67.47; H, 5.03; N, 17.49, found: C, 67.76; H, 4.71; N, 17.21.

N-(3-Butylthiazolo[4,5-b]quinoxalin-2(3H)-ylidene)aniline (5f) Yield 81 %; m.p.; 175 - 177 °C; IR (KBr,cm^{-1}): 3080 (CH arom.), 2885, 2810 (CH aliph.), 1688 (C=N); ^{1}H NMR (DMSO-d_6, δ, ppm): 1.23 (t, 3H, CH_3, $J = 16.20$ Hz), 1.26 - 1.38 (m, 2H, CH_2-CH_3), 1.69 - 1.79 (m, 2H, CH_2-CH_2-CH_3), 4.01 (t, 2H, N-CH_2, J = 7.08 Hz), 7.43 – 7.88 (m, 9H, Ar-H). ^{13}C NMR (DMSO-d_6, δ, ppm): 12.78 (CH_3), 20.81 (CH_2-CH_3), 28.52 (CH_2-CH_2-CH_3), 41.07 (N-CH_2-CH_2), 122.03 (2), 123.52, 126.33, 129.88, 129.98, 130.38, 132.07 (2), 136.15 (N=C-S), 136.31, 136.58, 149.04 (C-N), 157.16 (C=N), 161.89 (N=C-N). MS (m/z): 334 (M^+). Analysis calculated for: $C_{19}H_{18}N_4S$ (334): C, 68.23; H, 5.42; N, 16.75, found: C, 68.05; H, 5.73; N, 16.97.

N-(3-Isobutylthiazolo[4,5-b]quinoxalin-2(3H)-ylidene)aniline (5g) Yield 77 %; m.p.; 187 -189 °C; IR (KBr,cm^{-1}): 3055 (CH arom.), 2925, 2815 (CH aliph.), 1655 (C=N); ^{1}H NMR (DMSO-d_6, δ, ppm): 1.12 (d, 6H, $2CH_3$, $J = 3.24$ Hz), 2.13–2.20 (m, H, CH), 4.16 (d, 2H, CH_2-N, $J = 8.96$ Hz), 7.28 (d, 2H, Ar-H, $J = 7.88$ Hz), 7.54 (t, H, Ar-H, $J = 6.40$ Hz), 7.73-7.99 (m, 6H, Ar-H). ^{13}C NMR (DMSO-d_6, δ, ppm): 20.56 (2) (2 CH_3), 24.14 (CH_3-CH-CH_3), 54.39 (N-CH_2-CH), 123.74 (2), 126.32, 126.40, 129.91, 130.01, 130.44, 133.95 (2), 136.22 (N=C-S), 136.31, 136.65, 150.69 (C-N), 157.55 (C=N), 161.97 (N=C-N). MS (m/z): 334 (M^+). Analysis calculated for: $C_{19}H_{18}N_4S$ (334): C, 68.23; H, 5.42; N, 16.75, found: C, 67.94; H, 5.57; N, 16.93.

Ethyl 2-(phenylimino)thiazolo[4,5-b]quinoxaline-3(2H)-carboxylate (5h) Yield 92 %; m.p.; 194 - 196°C; IR (KBr,cm^{-1}): 3055 (CH arom.), 2910, 2840 (CH aliph.), 1670 (C=N); ^{1}H NMR (DMSO-d_6, δ, ppm): 1.29 (t, 3H, CH_3, $J = 7.08$ Hz), 4.12 (q, 2H, CH2, $J = 13.76$ Hz), 7.24 – 7.30 (m, 3H, Ar-H), 7.63 – 7.84 (m, 6H, Ar-H). ^{13}C NMR (DMSO-d_6, δ, ppm): 14.66 (CH_3), 60.96 (CH_2-CH_3), 122.20 (2), 124.73, 124.92, 129.90, 130.02, 130.44, 130.77 (2), 136.20 (N=C-S), 136.32, 136.63, 149.56 (C-N), 155.42 (C=O), 156.05 (C=N), 161.16 (N = C-N). MS (m/z): 350 (M^+). Analysis calculated for: $C_{18}H_{14}N_4O_2S$ (350): C, 61.70; H, 4.03; N, 15.99, found: C, 61.54; H, 4.16; N, 16.26.

N-(3-Cyclohexylthiazolo[4,5-b]quinoxalin-2(3H)-ylidene)aniline (5i) Yield 89 %; m.p.; 239–241 °C; IR (KBr,cm^{-1}): 3077 (CH arom.), 2896, 2813 (CH aliph.), 1667 (C=N); ^{1}H NMR (DMSO-d_6, δ, ppm): 1.19–1.32 (m, 6H, $3CH_2$-cyclohexane), 1.68–1.74 (m, 4H, $2CH_2$-cyclohexane), 2.89–2.98 (m, H, CH-cyclohexane), 7.58–7.88 (m, 9H, Ar-H). ^{13}C NMR (DMSO-d_6, δ, ppm): 26.41 (2) (2 CH_2-Cyclohexane), 26.65 (CH_2-Cyclohexane), 30.74 (2) (2 CH_2-Cyclohexane), 64.31 (N-CH_2-Cyclohexane), 124.76 (2), 126.33, 126.40, 129.94, 130.02, 130.42, 131.38 (2), 136.16 (N=C-S), 136.38, 136.65, 148.77 (C-N), 156.62 (C=N), 161.87 (N=C-N). MS (m/z): 360 (M^+). Analysis calculated for: $C_{21}H_{20}N_4S$ (360): C, 69.97; H, 5.59; N, 15.54, found: C, 70.28; H, 5.31; N, 15.72.

N-(3-Benzylthiazolo[4,5-b]quinoxalin-2(3H)-ylidene)aniline (5j) Yield 94 %; m.p.; 260–162 °C; IR (KBr,cm^{-1}): 3086 (CH arom.), 2916, 2839 (CH aliph.), 1685 (C=N); ^{1}H NMR (DMSO-d_6, δ, ppm): 4.81 (s, 2H, CH_2), 7.41–7.49 (m, 3H, Ar-H), 7.59–7.95 (m, 11H, Ar-H). ^{13}C NMR (DMSO-d_6, δ, ppm): 49.62 (CH_2), 124.12 (2), 125.95, 126.31, 126.62, 126.87 (2), 127.91, 128.05, 129.73 (2), 129.92, 130.02 (2), 136.20 (N=C-S), 136.33, 136.64, 137.83, 148.76 (C-N), 157.39 (C=N), 162.16 (N=C-N). MS (m/z): 368 (M^+). Analysis calculated for: $C_{22}H_{16}N_4S$ (368): C, 71.71; H, 4.38; N, 15.21, found: C, 71.47; H, 4.54; N, 15.42.

Pharmacological/biological assays

In-vitro studies

VEGFR-2 enzyme inhibition assay The in-vitro VEGFR-2 (KDR) kinase activity was measured for all compounds using VEGFR-2 ELISA kit (BPS Bioscience, CA, USA) according to manufacturer's instructions. The results were expressed as IC50. According to the results obtained, compounds **5h** and **5d**, showing the highest inhibitory effect, were selected to be employed in the evaluation of in-vitro cytotoxic activity against RCC cell line.

Estimation of anti-cancer activity against transitional cell line

Cell culture T-24: Urinary bladder cancer (transitional cell carcinoma) was obtained from Nawah Scientific Inc., (Mokatam, Cairo, Egypt). Cells were kept in McCoy's media supplemented with 100 mg/mL streptomycin, 100 units/mL penicillin, and 10% heat-inactivated fetal bovine serum at 37 °C in a humidified, 5% (v/v) CO_2 atmosphere.

Cytotoxicity assay SRB assay was used to determine cell viability. In 96-well plates, aliquots of 100 L cell suspension (5x103cells) were incubated in incomplete media for 24 h. Another aliquot of 100 L media containing drugs at various concentrations was given to the cells. Cells were fixed 72 h after drug exposure by replacing media with 150 µL of 10% TCA and incubating at 4 °C for 1 h. After removing the TCA solution, the cells were washed five times with distilled water. Aliquots of 70 µL SRB solution (0.4%w/v) were added and incubated for 10 min in a dark place at room temperature. Plates were washed three times with 1% acetic acid and air-dried overnight. The protein-bound SRB stain was then dissolved in 150 µL of TRIS (10 mM), and the absorbance was measured at 540 nm using a BMGLABTECH®-FLUOstarOmega microplate reader (Ortenberg, Germany). The experiment was carried out in triplicate. The data was calculated as a percentage of cell viability, and the concentration required to inhibit cell viability by 50% (IC50) was calculated. According to the present results, compound **5h** showed a potent cytotoxix activity againt renal tumor cells and was selected to be more validated by in-vivo study.

In-vivo study

Animals

Male albino Swiss mice weighing 25–30 g, were sourced from the animal breeding facility of the National Center for Radiation Research and Technology (NCRRT). Animals were acclimatized for at least one week before experiment in the animal facility of NCRRT. They were allowed to feed on laboratory chow and water ad libitum. The in-vivo study was performed according to the guidelines set by the Research Ethics Committee at the NCRRT (permit number: 4 A/ 22).

Irradiation

Animals received an acute dose of 8 Gy as whole body irradiation [47, 48]. Irradiation was carried at the NCRRT using the Gamma Cell-40 biological irradiator with a $Cesium^{137}$ source (Atomic Energy of Canada Ltd; Sheridan Science and Technology Park, Mississauga, Ontario, Canada). The radiation dose rate was 0.33 Gy/min.

Experimental design

To monitor the safety of compound **5h** before induction of the main experiment, a group of mice ($n = 6$) administered compound **5h** orally at an equivalent dose to that of the sorafenib for the same time interval of the main experiment and no mortality rate was recorded.

After that, mice were randomly allocated into 4 groups ($n = 6$), **Group I:** mice received saline and served as normal group, **Group II**: mice were exposed to radiation at a dose level of 8 Gy [IR] and received saline. This group served as irradiated control group, **Group III**: irradiated mice received sorafenib (50 mg/kg) [IR + sorafenib] as a reference drug [49], **Group IV**: irradiated mice received compound **5h** [IR + compound 5 h] at an equivalent dose to that of the sorafenib. Treatments were orally administered daily for 3 consecutive days, starting 1 h after irradiation.

The experiment was terminated three days after irradiation and mice were sacrificed by decapitation under urethane anesthesia. The blood samples were collected; serum was separated by cooling centrifugation at 4000 rpm at 4 °C for 10 min and stored at −80 °C for later use in estimating kidney functions. Afterward, kidneys were dissected, washed with saline, and homogenized in ice-cold PBS (PH 7.4) using Glas Col® homogenizer (Terre Haute, IN, USA). The homogenate were centrifuged at 4000 rpm at 4 °C for 10 min and the supernatants were then stored at −80 °C to be employed for biochemical tissue analysis. Kidneys from each group were kept in 10% formalin for further use in histopathological evaluation.

Assessment of kidney functions

Serum urea and creatinine were estimated *via* colorimetric method using commercially available kits (Biodiagnostic, Cairo, Egypt). The analysis was carried out according to the manufacturer's instructions and the absorbance of each sample was measured using Unicam 8625 UV/V spectrophotometer (Cambridge, UK).

Assessment of Kidney total protein

The kidney protein content was measured using Lowry et al. [50] technique with bovine serum albumin as the reference protein.

Assessment of pro-angiogenic, pro-fibrotic and apoptotic markers

The concentrations of VEGFR-2 (pro-angiogenic), TGF-β1 (pro-fibrotic) and caspase-3 (apoptotic) were estimated in kidney tissue by ELISA technique. Commercially available kits for the determination of VEGFR-2 was purchased from Elabscience (Texas, USA, Catalog no: E-El-R01053), that for TGF-β1 was purchased from Cell Sciences (Massachusetts, USA, Catalog no: 670.070.128) and that for caspase-3 was purchased from Cusabio Technology LLC (Houston, USA, Catalog no: CSB-E07264r). The analysis was carried out according to the manufacturer's instructions. An ELISA plate reader

Dynatec MR5000 (Guernsey, Channel Island, UK) was employed to measure the absorbance of each sample. Values are expressed as ng/mg protein.

Histopathological examinations

Kidney tissue samples were fixed in 10% formol saline before being trimmed, washed, and dehydrated in increasing grades of alcohol. The dehydrated specimens were then cleared in xylene, embedded in paraffin blocks, and sectioned at a thickness of 4-6 m. For histopathological examination using an electric light microscope, the tissue sections were deparaffinized with xylol and stained with hematoxylin and eosin (H&E) [51]. Adobe Photoshop was used to capture and process the images (version 8). Histopathological examinations were carried out in blind fashion. The frequency and severity of kidney lesions were evaluated semi-quantitatively using a scale of 0 to 5, based on the severity of tubular cell necrosis, apoptosis, and degeneration [52].

Statistical analysis

All data were expressed as mean values ± standard error of the mean (SEM). The Kolmogorov-Smirnov test was used to confirm data normality, and all data had a normal distribution. One-way analysis of variance (ANOVA) was used to compare different groups, followed by the Tukey-Kramer multiple comparison test. Graph Pad prism 5 was used for statistical analysis (Graph Pad Software Inc, San Diego, California, USA). A p value less than 0.05 was deemed significant. For figure representation, Microsoft Excel programme was used.

Molecular docking

The molecular docking study for compound 5 h's structure was carried out using the Molecular Operating Environment (MOE) software, version 2014.090. The energy of the compound was minimised using the HamiltonianForce FieldMMFF94x. The partial charges of the forcefield were computed. The conformational stochastic of compound 5 h was analysed using the default settings. The X-ray crystal structure of VEGFR-2 in complex with sorafenib as ligand (PDB ID: 4ASD) was obtained from http://www.rscb.org/pdb. The Protein Data Bank (pdb) protein-ligand complex was prepared for docking. After threedimensional protonation of the enzyme, the system was optimised. Protein repeated chains and co-crystallized water molecules were removed. The binding pocket was determined and isolated, and the backbone was then hidden. The results were validated by redocking the sorafenib ligand. MOEDOCK was used to determine the most stable conformers' flexible docking of the ligandrigid receptor. The alpha triangle placement method and London dG as a function were used for scoring. Using the same scoring function, forcefield refinement was applied to the obtained poses. 50 of the most stable docking models of the ligand with the highest scored conformation were retained.

Acknowledgements We would like to thank the staff members of the γ-irradiation unit at the National Center for Radiation Research and Technology (NCRRT) for their cooperation in carrying out the irradiation.

Funding Open access funding provided by The Science, Technology & Innovation Funding Authority (STDF) in cooperation with The Egyptian Knowledge Bank (EKB).

Compliance with ethical standards

Conflict of interest The authors declare no competing interests.

Publisher's note Springer Nature remains neutral with regard to jurisdictional claims in published maps and institutional affiliations.

References

1. Bhatt JR, Finelli A. Landmarks in the diagnosis and treatment of renal cell carcinoma. Nat Rev Urol. 2014;11:517–25. https://doi.org/10.1038/nrurol.2014.194
2. De Felice F, Tombolini V. Radiation therapy in renal cell carcinoma. Crit Rev Oncol Hematol. 2018;128:82–7. https://doi.org/10.1016/j.critrevonc.2018.06.002
3. Klaus R, Niyazi M, Lange-Sperandio B. Radiation-induced kidney toxicity: molecular and cellular pathogenesis. Radiat Oncol. 2021;16:43 https://doi.org/10.1186/s13014-021-01764-y
4. Fiore M, D Apos Angelillo RM, Greco C, Fioroni I, Ippolito E, Santini D, et al. Radiotherapy and vascular endothelial growth factor receptor-tyrosine kinase inhibitors in renal cancer. Chemotherapy. 2018;63:83–9. https://doi.org/10.1159/000488252
5. Choueiri TK, Kaelin WG Jr. Targeting the HIF2-VEGF axis in renal cell carcinoma. Nat Med. 2020;26:1519–30. https://doi.org/10.1038/s41591-020-1093-z
6. Escudier B, Eisen T, Stadler WM, Szczylik C, Oudard S, Siebels M, et al. Sorafenib in advanced clear-cell renal-cell carcinoma. N. Engl J Med. 2007;356:125–34. https://doi.org/10.1056/NEJMoa060655
7. Antoun S, Baracos VE, Birdsell L, Escudier B, Sawyer MB. Low body mass index and sarcopenia associated with dose-limiting toxicity of sorafenib in patients with renal cell carcinoma. Ann Oncol. 2010;21:1594–8. https://doi.org/10.1093/annonc/mdp605

8. Dizman N, Philip EJ, Pal SK. Genomic profiling in renal cell carcinoma. Nat Rev Nephrol. 2020;16:435–51. https://doi.org/10.1038/s41581-020-0301-x
9. Lalani AA, Heng DYC, Basappa NS, Wood L, Iqbal N, Mcleod D, et al. Evolving landscape of first-line combination therapy in advanced renal cancer: a systematic review. Ther Adv Med Oncol. 2022;14:17588359221108685 https://doi.org/10.1177/17588359221108685
10. Liu Y, Li Y, Wang Y, Lin C, Zhang D, Chen J, et al. Recent progress on vascular endothelial growth factor receptor inhibitors with dual targeting capabilities for tumor therapy. J Hematol Oncol. 2022;15:89 https://doi.org/10.1186/s13045-022-01310-7
11. Makhov P, Joshi S, Ghatalia P, Kutikov A, Uzzo RG, Kolenko VM. Resistance to systemic therapies in clear cell renal cell carcinoma: mechanisms and management strategies. Mol Cancer Ther. 2018;17:1355–64. https://doi.org/10.1158/1535-7163.Mct-17-1299
12. He Y, Luo Y, Huang L, Zhang D, Wang X, Ji J, et al. New frontiers against sorafenib resistance in renal cell carcinoma: From molecular mechanisms to predictive biomarkers. Pharm Res. 2021;170:105732 https://doi.org/10.1016/j.phrs.2021.105732
13. Bala Aakash V, Ramalakshmi N, Bhuvaneswari S, Sankari E, Arunkumar S. Comprehensive Review on Versatile Pharmacology of Quinoxaline Derivative. Russ J Bioorg Chem. 2022;48:657–77. https://doi.org/10.1134/S1068162022040069
14. Khatoon H, Abdulmalek E. Novel synthetic routes to prepare biologically active quinoxalines and their derivatives: a synthetic review for the last two decades. Molecules. 2021;26:1055 https://doi.org/10.3390/molecules26041055
15. Pinheiro AC, Mendonça Nogueira TC, De Souza MV. Quinoxaline nucleus: a promising scaffold in anti-cancer drug discovery. Anticancer Agents Med Chem. 2016;16:1339–52. https://doi.org/10.2174/1871520616666160622090839
16. Montana M, Mathias F, Terme T, Vanelle P. Antitumoral activity of quinoxaline derivatives: a systematic review. Eur J Med Chem. 2019;163:136–47. https://doi.org/10.1016/j.ejmech.2018.11.059
17. Alanazi MM, Elkady H, Alsaif NA, Obaidullah AJ, Alanazi WA, Al-Hossaini AM, et al. Discovery of new quinoxaline-based derivatives as anticancer agents and potent VEGFR-2 inhibitors: Design, synthesis, and in silico study. J Mol Struct. 2022;1253:132220 https://doi.org/10.1016/j.molstruc.2021.132220
18. El-Gazzar MG, El-Hazek RM, Zaher NH, El-Ghazaly MA. Design and synthesis of novel pyridazinoquinazoline derivatives as potent VEGFR-2 inhibitors: In vitro and in vivo study. Bioorg Chem. 2019;92:103251 https://doi.org/10.1016/j.bioorg.2019.103251
19. Rini BI. Vascular endothelial growth factor-targeted therapy in renal cell carcinoma: current status and future directions. Clin Cancer Res. 2007;13:1098–106. https://doi.org/10.1158/1078-0432.Ccr-06-1989
20. Mohamed TK, Batran RZ, Elseginy SA, Ali MM, Mahmoud AE. Synthesis, anticancer effect and molecular modeling of new thiazolylpyrazolyl coumarin derivatives targeting VEGFR-2 kinase and inducing cell cycle arrest and apoptosis. Bioorg Chem. 2019;85:253–73. https://doi.org/10.1016/j.bioorg.2018.12.040
21. Keating GM. Axitinib: a review in advanced renal cell carcinoma. Drugs. 2015;75:1903–13. https://doi.org/10.1007/s40265-015-0483-x
22. Bronte E, Galvano A, Novo G, Russo A. Cardiotoxic effects of anti-VEGFR tyrosine kinase inhibitors. In Cardio-Oncology: Principles, Prevention and Management. Elsevier Inc. 2016; 69–89.
23. Alsaif NA, Dahab MA, Alanazi MM, Obaidullah AJ, Al-Mehizia AA, Alanazi MM, et al. New quinoxaline derivatives as VEGFR-2 inhibitors with anticancer and apoptotic activity: Design, molecular modeling, and synthesis. Bioorg Chem. 2021;110:104807 https://doi.org/10.1016/j.bioorg.2021.104807
24. Lee K, Jeong KW, Lee Y, Song JY, Kim MS, Lee GS, et al. Pharmacophore modeling and virtual screening studies for new VEGFR-2 kinase inhibitors. Eur J Med Chem. 2010;45:5420–7. https://doi.org/10.1016/j.ejmech.2010.09.002
25. Yu P, Ye L, Wang H, Du G, Zhang J, Zhang J, et al. NSK-01105 inhibits proliferation and induces apoptosis of prostate cancer cells by blocking the Raf/MEK/ERK and PI3K/Akt/mTOR signal pathways. Tumour Biol. 2015;36:2143–53. https://doi.org/10.1007/s13277-014-2824-x
26. Chen F, Fang Y, Zhao R, Le J, Zhang B, Huang R, et al. Evolution in medicinal chemistry of sorafenib derivatives for hepatocellular carcinoma. Eur J Med Chem. 2019;179:916–35. https://doi.org/10.1016/j.ejmech.2019.06.070
27. Pascal J-C, Pinhas H, Laure F, Dumez D, Poizot A. New antiarrhythmic agents: piperazine guanidine derivatives. Eur J Med Chem. 1990;25:81–5.
28. Viana GM, Soares DC, Santana MV, Do Amaral LH, Meireles PW, Nunes RP, et al. Antileishmanial thioureas: synthesis, biological activity and in silico evaluations of new promising derivatives. Chem Pharm Bull. 2017;65:911–9. https://doi.org/10.1248/cpb.c17-00293
29. Mandal S, Pramanik A. Facile synthesis of phthalidyl fused spiro thiohydantoins through silica sulfuric acid induced oxidative rearrangement of ninhydrin adducts of thioureas. Tetrahedron. 2020;76:130817 https://doi.org/10.1016/j.tet.2019.130817
30. Wei TB, Lin Q, Zhang YM, Wang H. Efficient and novel Synthesis of N-Aryl-N′-ethoxycarbonylthiourea and arene-bis-ethoxycarbonylthiourea derivatives catalyzed by TMEDA. Synth Commun. 2004;34:2205–13. https://doi.org/10.1081/SCC-120038502
31. El-Adl K, El-Helby AA, Sakr H, Eissa IH, El-Hddad SSA, MIaS F. Design, synthesis, molecular docking and anticancer evaluations of 5-benzylidenethiazolidine-2,4-dione derivatives targeting VEGFR-2 enzyme. Bioorg Chem. 2020;102:104059 https://doi.org/10.1016/j.bioorg.2020.104059
32. Abuelizz HA, Marzouk M, Bakheit AH, Awad HM, Soltan MM, Naglah AM. et al.Antiproliferativeand antiangiogenic properties of new VEGFR-2-targeting2-thioxobenzo[g]quinazoline derivatives (in vitro).Molecules.2020;25:5944.https://doi.org/10.3390/molecules25245944.
33. Sánchez-Gastaldo A, Kempf E, González Del Alba A, Duran I. Systemic treatment of renal cell cancer: a comprehensive review. Cancer Treat Rev. 2017;60:77–89. https://doi.org/10.1016/j.ctrv.2017.08.010
34. Hajri M, Esteve MA, Khoumeri O, Abderrahim R, Terme T, Montana M, et al. Synthesis and evaluation of in vitro antiproliferative activity of new ethyl 3-(arylethynyl)quinoxaline-2-carboxylate and pyrido[4,3-b]quinoxalin-1(2H)-one derivatives. Eur J Med Chem. 2016;124:959–66. https://doi.org/10.1016/j.ejmech.2016.10.025
35. Anscher MS, Chen L, Rabbani Z, Kang S, Larrier N, Huang H, et al. Recent progress in defining mechanisms and potential targets for prevention of normal tissue injury after radiation therapy. Int J Radiat Oncol Biol Phys. 2005;62:255–9. https://doi.org/10.1016/j.ijrobp.2005.01.040
36. Dent P, Reardon DB, Park JS, Bowers G, Logsdon C, Valerie K, et al. Radiation-induced release of transforming growth factor alpha activates the epidermal growth factor receptor and mitogen-activated protein kinase pathway in carcinoma cells, leading to increased proliferation and protection from radiation-induced cell death. Mol Biol Cell. 1999;10:2493–506. https://doi.org/10.1091/mbc.10.8.2493
37. Gorski DH, Beckett MA, Jaskowiak NT, Calvin DP, Mauceri HJ, Salloum RM, et al. Blockage of the vascular endothelial growth factor stress response increases the antitumor effects of ionizing radiation. Cancer Res. 1999;59:3374–8.
38. Talebpour Amiri F, Hamzeh M, Naeimi RA, Ghasemi A, Hosseinimehr SJ. Radioprotective effect of atorvastatin against ionizing

radiation-induced nephrotoxicity in mice. Int J Radiat Biol. 2018;94:106–13. https://doi.org/10.1080/09553002.2018.1420926
39. Prise KM, Schettino G, Folkard M, Held KD. New insights on cell death from radiation exposure. Lancet Oncol. 2005;6:520–8. https://doi.org/10.1016/s1470-2045(05)70246-1
40. Soliman AF, Saif-Elnasr M, Abdel Fattah SM. Platelet-rich plasma ameliorates gamma radiation-induced nephrotoxicity via modulating oxidative stress and apoptosis. Life Sci. 2019;219:238–47. https://doi.org/10.1016/j.lfs.2019.01.024
41. Özyurt H, Çevik Ö, Özgen Z, Özden AS, Çadırcı S, Elmas MA, et al. Quercetin protects radiation-induced DNA damage and apoptosis in kidney and bladder tissues of rats. Free Radic Res. 2014;48:1247–55. https://doi.org/10.3109/10715762.2014.945925
42. Jackson IL, Chen L, Batinic-Haberle I, Vujaskovic Z. Superoxide dismutase mimetic reduces hypoxia-induced O2*-, TGF-beta, and VEGF production by macrophages. Free Radic Res. 2007;41:8–14. https://doi.org/10.1080/10715760600913150
43. Zhao ZM, Liu HL, Sun X, Guo T, Shen L, Tao YY, et al. Levistilide A inhibits angiogenesis in liver fibrosis via vascular endothelial growth factor signaling pathway. Exp Biol Med (Maywood). 2017;242:974–85. https://doi.org/10.1177/1535370217701005
44. Yang T, Vesey DA, Johnson DW, Wei MQ, Gobe GC. Apoptosis of tubulointerstitial chronic inflammatory cells in progressive renal fibrosis after cancer therapies. Transl Res. 2007;150:40–50. https://doi.org/10.1016/j.trsl.2007.01.006
45. Mostafa NM, Edmond MP, El-Shazly M, Fahmy HA, Sherif NH, Singab ANB. Phytoconstituents and renoprotective effect of Polyalthia longifolia leaves extract on radiation-induced nephritis in rats via TGF-β/smad pathway. Nat Prod Res. 2022;36:4187–92. https://doi.org/10.1080/14786419.2021.1961252
46. Ghorab MM, Osman AN, Noaman E, Heiba HI, Zaher NH. The Synthesis of some new sulfur heterocyclic compounds as potential radioprotective and anticancer agents. Phosphorus Sulfur Silicon Relat Elem. 2006;181:1935–50. https://doi.org/10.1080/10426500500544014
47. Kunwar A, Verma P, Bhilwade HN, Iwaoka M, Priyadarsini KI. Dihydroxyselenolane (DHS) supplementation improves survival following whole-body irradiation (WBI) by suppressing tissue-specific inflammatory responses. Mutat Res Genet Toxicol Environ Mutagen. 2016;807:33–46. https://doi.org/10.1016/j.mrgentox.2016.07.002
48. Saberi H, Keshavarzi B, Shirpoor A, Gharalari FH, Rasmi Y. Rescue effects of ginger extract on dose dependent radiation-induced histological and biochemical changes in the kidneys of male Wistar rats. Biomed Pharmacother. 2017;94:569–76. https://doi.org/10.1016/j.biopha.2017.07.128
49. Wei J, Liu R, Zhang J, Liu S, Yan D, Wen X, et al. Baicalin enhanced oral bioavailability of sorafenib in rats by inducing intestine absorption. Front Pharm. 2021;12:761763 https://doi.org/10.3389/fphar.2021.761763
50. Lowry OH, Rosebrough NJ, Farr AL, Randall RJ. Protein measurement with the Folin phenol reagent. J Biol Chem. 1951;193:265–75.
51. Bancroft JD, Stevens A, Turner DR. Theory and practice of histological techniques. New York, London, San Francisco, Tokyo: Churchill Livingstone; 2013.
52. Zhang J, Brown RP, Shaw M, Vaidya VS, Zhou Y, Espandiari P, et al. Immunolocalization of Kim-1, RPA-1, and RPA-2 in kidney of gentamicin-, mercury-, or chromium-treated rats: relationship to renal distributions of iNOS and nitrotyrosine. Toxicol Pathol. 2008;36:397–409. https://doi.org/10.1177/0192623308315832